CARDIAC IMAGING

Accurate needle-free assessment of myocardial oxygenation for ischemic heart disease in canines using magnetic resonance imaging

Hsin-Jung Yang[1,2], Ilkay Oksuz[3], Damini Dey[1,2], Jane Sykes[4], Michael Klein[5], John Butler[4], Michael S. Kovacs[4], Olivia Sobczyk[5], Ivan Cokic[1], Piotr J. Slomka[1,2], Xiaoming Bi[6], Debiao Li[1,2], Mourad Tighiouart[1], Sotirios A. Tsaftaris[7], Frank S. Prato[4], Joseph A. Fisher[5], Rohan Dharmakumar[1,2]*

Myocardial oxygenation—the ability of blood vessels to supply the heart muscle (myocardium) with oxygen—is a critical determinant of cardiac function. Impairment of myocardial oxygenation is a defining feature of ischemic heart disease (IHD), which is caused by pathological conditions that affect the blood vessels supplying oxygen to the heart muscle. Detecting altered myocardial oxygenation can help guide interventions and prevent acute life-threatening events such as heart attacks (myocardial infarction); however, current diagnosis of IHD relies on surrogate metrics and exogenous contrast agents for which many patients are contraindicated. An oxygenation-sensitive cardiac magnetic resonance imaging (CMR) approach used previously to demonstrate that CMR signals can be sensitized to changes in myocardial oxygenation showed limited ability to detect small changes in signals in the heart because of physiologic and imaging noise during data acquisition. Here, we demonstrate a CMR-based approach termed cfMRI [cardiac functional magnetic resonance imaging (MRI)] that detects myocardial oxygenation. cfMRI uses carbon dioxide for repeat interrogation of the functional capacity of the heart's blood vessels via a fast MRI approach suitable for clinical adoption without limitations of key confounders (cardiac/respiratory motion and heart rate changes). This method integrates multiple whole-heart images within a computational framework to reduce noise, producing confidence maps of alterations in myocardial oxygenation. cfMRI permits noninvasive monitoring of myocardial oxygenation without requiring ionizing radiation, contrast agents, or needles. This has the potential to broaden our ability to noninvasively identify IHD and a diverse spectrum of heart diseases related to myocardial ischemia.

INTRODUCTION

Ischemic heart disease (IHD) is the leading cause of death in the Western world (*1*). It often stems from atherosclerotic narrowing of the coronary arteries (stenosis), leading to reduced blood flow and oxygen supplied to the heart muscle (myocardium). This causes myocardial ischemia during physical exertion, a condition where the oxygen supply to the heart muscle does not meet the myocardial oxygen demand (*2*). The presence and extent of myocardial ischemia are key predictors of major adverse cardiac events (MACEs), including stroke, heart attack (myocardial infarction), and death (*1*). Early interventions (medical, surgical, or lifestyle), guided by the extent and severity of ischemia, are crucial for reducing MACEs in IHD patients (*3*–*5*). Yet, to date, there are no reliable noninvasive methods to evaluate the presence or severity of deficiencies in meeting myocardial oxygen demands.

Given the lack of viable methods to assess myocardial oxygenation, the diagnosis of IHD has become entrenched in the use of surrogate metrics, notably electrocardiography (ECG) or myocardial blood flow (MBF). Among these, the determination of ongoing myocardial ischemia based on ECG changes is attractive because ECG assessment is highly accessible. However, ECG may be nonspecific, can be normal in patients during an ischemic event, and cannot identify asymptomatic patients with marked coronary stenosis unless combined with exercise stress, which is not tolerated by more than 50% of IHD patients (*6*).

Methods based on MBF are the most widely used for the assessment of IHD and recommended by the American Heart Association (AHA). MBF changes can be determined using several clinically available imaging methods, including single-photon emission computed tomography (SPECT), positron emission tomography (PET), first-pass perfusion cardiac magnetic resonance imaging (CMR), and contrast-enhanced echocardiography (*7*). These methods are often combined with exercise stress or intravenously injected stress agent (adenosine) to assess the extent and severity of ischemic burden. However, these methods have limited diagnostic capabilities: For example, SPECT and PET approaches are used in more than 90% of the nearly 10 million myocardial ischemia-testing studies in the United States (*1*), but they require radioactive tracers, which pose incremental risk to patients (*8*). Other methods, such as first-pass perfusion CMR, are free of ionizing radiation but require intravenously delivered exogenous contrast media, based on gadolinium (*7*), which are contraindicated in patients with chronic kidney disease (*9*). More recently, a T_1-based magnetic resonance imaging (MRI) method that does not require exogenous contrast agents or ionizing radiation, likely based on impairments in myocardial blood volume, has been demonstrated in patients with IHD (*10*). However, because oxygen supply and demand to a given physiological stimulus are variable in every patient, assessment of MBF or myocardial blood volume may not provide full physiological insight into the extent and severity of myocardial ischemia in patients with IHD (*11*). Furthermore, there are pathological conditions in which perfusion is normal but oxygenation is impaired (*12*, *13*). For these reasons, a noninvasive method of measuring myocardial oxygenation is preferable.

To assess IHD based on myocardial oxygenation without ionizing radiation or exogenous contrast media, blood oxygen level–dependent (BOLD) cardiac MRI (BOLD-CMR) has been investigated (*14*). The

[1]Cedars-Sinai Medical Center, Los Angeles, CA 90048, USA. [2]University of California, Los Angeles CA 90095, USA. [3]King's College London, London WC2R 2LS, UK. [4]Lawson Health Research Institute, University of Western Ontario, London, ON N6C 2R5, Canada. [5]University of Toronto and University Health Network, Toronto, ON M5G 2C4, Canada. [6]MR R&D Collaborations, Siemens Healthineers, Los Angeles, CA 90048, USA. [7]School of Engineering, University of Edinburgh, EH8 9YL, UK.
*Corresponding author. Email: rohandkumar@csmc.edu

evidence that BOLD-CMR changes are primarily a reflection of myocardial oxygenation was presented nearly two decades ago (*15*, *16*), leading to several pilot clinical validation studies that tested the method's feasibility (*12*, *17*, *18*). However, the state-of-the-art BOLD-CMR approach has been shown to perform poorly against the current "state of the art" PET (*12*). It is not known whether this discrepancy is a true difference between a test for myocardial oxygenation and a test for MBF, or whether it is a consequence of known accuracy limitations of BOLD-CMR. Without a reliable approach to assess myocardial oxygenation, there is no way to directly evaluate the method's status in IHD, its relationship to MBF, and its potential for diagnosis for new, "at-risk" patients, in whom impaired oxygenation does not accompany detectable abnormalities in blood flow.

Uncertainty of a measurement is fundamentally determined by noise. In BOLD-CMR, physiological noise (motion) and imaging noise (limitations in signal reception elements, termed "radiofrequency coils") dominate the small signal changes that result from oxygenation changes. This makes it challenging to accurately index an observed signal change against blood oxygenation. The realization that the uncertainty of a measured signal can be reduced if the response can be repeatedly modulated by a known stimulus (*19*) was a major breakthrough for BOLD-CMR in the brain (functional MRI, abbreviated as fMRI) and it enabled sensitivity required for accurate detection of oxygenation changes, which has advanced our understanding of neural processes over the past two decades (*20*). Although this approach for defeating the critical noise limitations of BOLD-CMR is appealing, translating it into practice for myocardial oxygenation assessment is complex. Unlike in the brain, where the vasoactive stimulus is easily repeatable because it is visual or cognitive, injectable drugs such as adenosine are used to stimulate changes in the heart and these cannot be repeatedly administered within the same examination due to adverse side effects (*21*). To statistically uncover the underlying BOLD-CMR signals in the heart, rapidly acquired images registered across multiple stimulations, as well as whole-heart BOLD-CMR images, are required. However, state-of-the art BOLD-CMR is essentially two-dimensional (2D): It is typically limited to a single slice, because whole-heart 3D acquisitions that are sensitive to oxygenation cannot be completed within the time that pharmacological agents are administered. The current acquisition schemes are also sensitive to heart rate variations between different vasodilatory states. This means that they can contaminate the BOLD-CMR signal readouts by masking the signal associated with true physiological changes in blood flow and oxygenation.

Here, we show that advances in coronary vasodilation and data acquisition can overcome these challenges. Specifically, we demonstrate that healthy myocardium and tissue affected by coronary narrowing could be detected without contrast agents or ionizing radiation using repeat stimulation with increased arterial CO_2 ($PaCO_2$). To facilitate this, we performed rapid whole-heart imaging using a free-breathing BOLD-CMR approach in canines and integrated registered and segmented images to generate statistical parametric maps (SPMs). This cardiac fMRI (cfMRI) approach can potentially enable noninvasive examination of IHD without ionizing radiation, exogenous contrast agents, or intravenous stress agents.

RESULTS

Repeat stimulation enables robust myocardial BOLD-CMR: Proof of concept using 2D BOLD-CMR

Previous studies have shown that arterial CO_2 tension, when increased by 25 mmHg from baseline, can accentuate MBF by more than twofold [a hallmark of potent coronary vasodilators (*22*)], and that such changes can be identified with 2D myocardial BOLD-CMR. However, studies to determine whether repeat exposure of the heart to a predefined CO_2 stimulus can be used to improve the detection of healthy and hypoperfused myocardium with or without coronary stenosis have not been reported. To fill this gap in knowledge, we first exposed dogs to repeat modulation of arterial CO_2 [normocapnia, end-tidal CO_2 ($PETCO_2$) = 35 mmHg; hypercapnia $PETCO_2$ = 60 mmHg] and free-breathing 2D BOLD-CMR to assess healthy myocardium in dogs (n = 5) without coronary stenosis using averaged BOLD responses. Next, we performed studies in the same dogs subjected to coronary stenosis (n = 5) to identify whether ischemic territories can be identified using signal averaging to reduce image noise. We validated our findings against simultaneously acquired ^{13}N-ammonia PET.

Typical results from healthy dogs (without coronary artery stenosis) exposed to intermittent hypercapnia (established with prospective control of $PaCO_2$; Fig. 1A) are shown in Fig. 1B. To investigate the dynamic myocardial BOLD response as a function of $PaCO_2$ in each myocardial segment, we acquired BOLD images of the midventricular myocardium, segmented images according to the AHA six-segment model, and measured the BOLD response in each segment (Fig. 1B). Every segment showed elevated BOLD response during the hypercapnic stimulations that were absent during normocapnia. When animals were subjected to repeat hypercapnia and normocapnia, the pattern of BOLD response was reproducible across all segments. Maps of BOLD response observed after administration of paired $PaCO_2$ modulation (defined as hypercapnia followed by normocapnia) demonstrate that average myocardial BOLD response derived after multiple stimulations was more homogeneous and higher in magnitude compared to a single stimulation (Fig. 1C). This observation was consistent with MBF changes observed with ^{13}N-ammonia PET (Fig. 1C).

To examine whether this approach could be used to improve the identification of myocardial territories subtended by coronary stenosis, we surgically controlled the left anterior descending coronary artery (LAD) diameter by adjusting the Doppler flow velocity of the vessel as previously described (*23*). Subsequently, we exposed each animal to multiple $PaCO_2$ stimulations during which time 2D BOLD-CMR and ^{13}N-ammonia PET scans were acquired. BOLD response observed in each segment of the midventricular myocardium (segmented according to the AHA recommendation) was measured. A typical BOLD response is shown in Fig. 1D. Myocardial BOLD response to hypercapnia was strong in segments 1 to 5, but not in segment 6 (Fig. 1D). Maps of BOLD response observed after the first $PaCO_2$ stimulation were relatively heterogeneous (Fig. 1E), but the average BOLD response after four repeat stimulations showed a confined region of impaired BOLD response consistent with the LAD territory (Fig. 1E), which was consistent with ^{13}N-ammonia PET (Fig. 1E).

Whole-heart myocardial BOLD-CMR with repeat hypercapnic stimulations

Although repeat hypercapnic stimulations combined with 2D BOLD-CMR and signal averaging can improve the visualization of standard, single-stimulation BOLD-CMR, there are practical limitations. First, with this approach, the BOLD responses need to be visually delineated, which introduces subjectivity into image analysis. Second, 2D CMR acquisition schemes are limited because of inadequate speed to fully

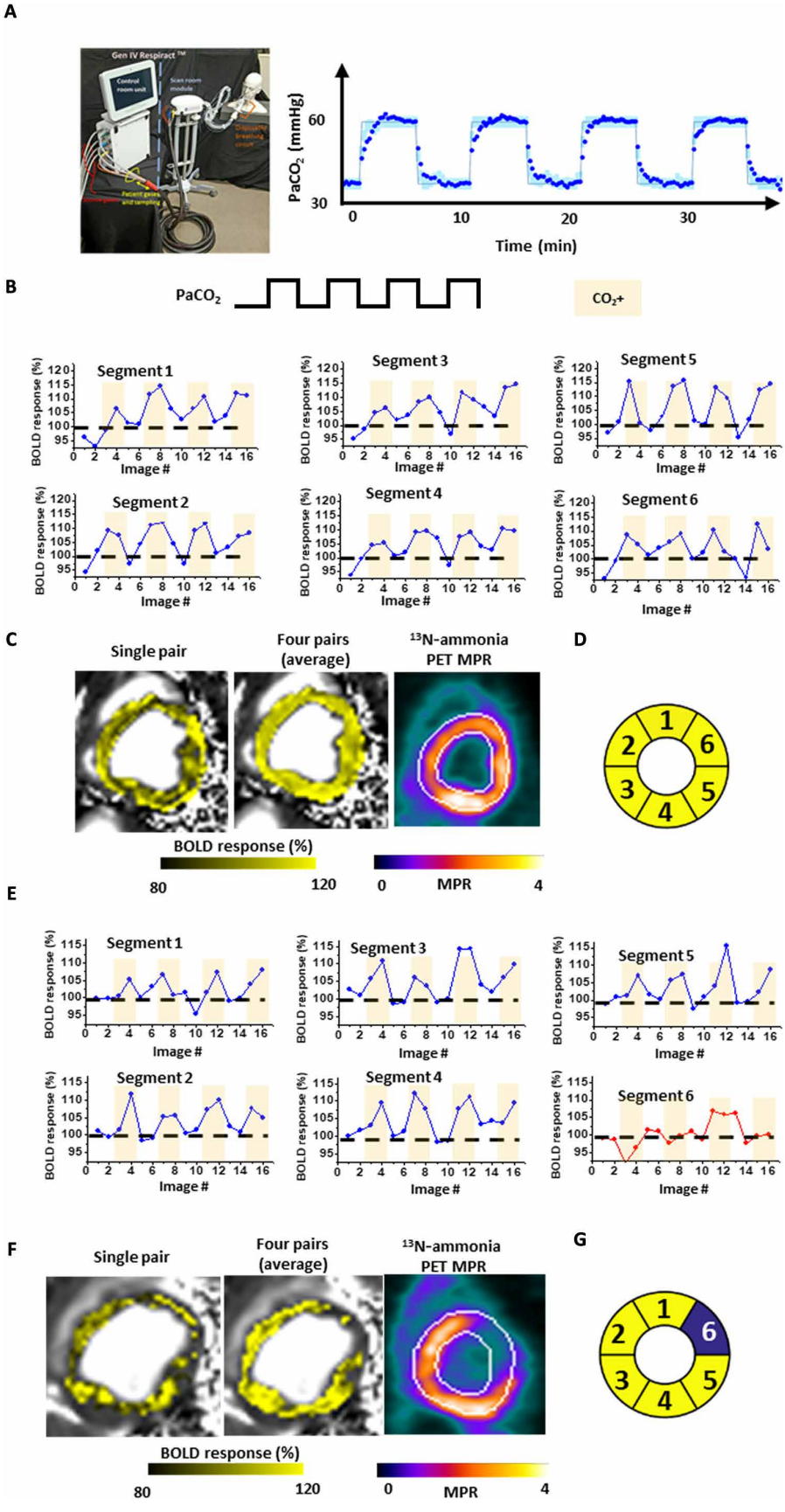

Fig. 1. Repeat stimulations and image averaging for enhancing myocardial BOLD response. (**A**) Prospective control of $PaCO_2$. The image (left) shows the system (computer-controlled gas control, input for source gases, and disposable breathing circuit) used for prospectively modulating $PaCO_2$. The graph (right) shows the trace of achieved $PaCO_2$ during the scans. Light blue trace represents the targeted $PETCO_2$, and dark blue points denote the actual $PETCO_2$ values. Representative results in a healthy dog during repeated intermittent hypercapnia (four stimulations) are presented in (B) to (D). (**B**) Representative segmental BOLD response in AHA segments 1 through 6 in a healthy dog during the first four blocks of intermittent hypercapnia (four stimulations). (**C**) Spatial distribution of the BOLD response in the midventricular myocardium after one hypercapnic stimulation (single pair, left) and mean BOLD response after four hypercapnic stimulations (four pairs, middle). The ^{13}N-ammonia PET response (MPR, right) was acquired simultaneously with BOLD-CMR. (**D**) Corresponding location of the AHA segments in a bullseye plot. Representative results in a dog with LAD coronary stenosis during repeated intermittent hypercapnia (four stimulations) are presented in (E) to (G). (**E**) Representative segmental BOLD response across AHA segments 1 through 6 during four blocks of intermittent hypercapnia (four stimulations) from an animal with LAD coronary stenosis. (**F**) Spatial maps of the BOLD response in the midventricular myocardium after one hypercapnic stimulation (left) and mean BOLD response after four hypercapnic stimulations (middle). The ^{13}N-ammonia PET response (MPR, right) was acquired simultaneously with BOLD-CMR. (**G**) Corresponding location of the AHA segments in a bullseye plot. The LAD territory highlighted with a blue shade indicates the presence of coronary stenosis.

image the heart multiple times to accommodate repeat hypercapnic stimulations; irrecoverable cardiac motion between multiple acquisitions leading to misregistration errors; and undesirable contributions from T_1 weighing, coil bias, breathing motion, and heart rate dependency, all of which confound the BOLD response. Collectively, these limitations can compromise both sensitivity and specificity of BOLD-CMR.

To address these limitations, we first performed numerical simulations by considering a range of peak BOLD signal responses and associated noise to estimate whether the confidence in detecting myocardial BOLD response can be improved by increasing the number of measurements in a statistical test using repeated-measures analysis of variance (ANOVA). The results (Fig. 2) showed that the statistical confidence ($P < 0.05$) in identifying the presence of a BOLD response is directly related to the maximal dynamic range of the response available and the number of repeat measurements. Specifically, it identified that more than three repeat measurements would

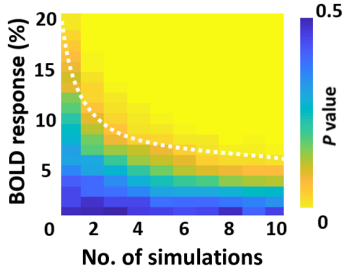

Fig. 2. Theoretical basis for objective assessment of myocardial BOLD response. Numerically simulated BOLD response according to the number of stimulations required to establish statistical significance (color-coded *P* values). For a given BOLD response, the number of stimulations required for reliable assessment ($P < 0.05$) of a change from baseline condition lies at the right of the white dotted line. For example, to reliably detect a BOLD response with a peak BOLD signal response of 10%, greater than three measurements are needed. The color bar on the right provides the scale for *P* values.

be needed to objectively identify the healthy myocardial territories for a given average myocardial BOLD response in the heart, which is typically ~10% (*23*). This model provided the basis for developing a statistical framework for objectively discriminating between myocardial regions that are responsive to a given stimulus from those that are not on the basis of repeat measurements. Next, we developed a fast, free-breathing, 3D T_2 mapping technique at a magnetic field strength of 3 T that is insensitive to heart rate changes between rest and stress states, to allow repeat imaging of the whole heart under multiple hypercapnic/normocapnic stimulations. We then performed in vivo studies in healthy canines ($n = 8$) under repeat hypercapnic/normocapnic stimulations. Subsequently, we analyzed the observed BOLD response within an ANOVA framework to derive SPMs of *P* values.

The framework of the data acquisition protocol, image acquisition and reconstruction strategy, and statistical analysis used to analyze the BOLD images is summarized in Fig. 3. We developed a data acquisition protocol under time-varying $PaCO_2$ (alternating between normocapnia and hypercapnia) (Fig. 3A). To rapidly image the whole heart under hypercapnic stimulation, a confounder-corrected T_2 CMR pulse sequence encompassing magnetization preparation, time-efficient *k*-space sampling, and motion-corrected T_2 mapping was developed (Fig. 3B). We used the T_2 values to assess the BOLD response. Figure 3C shows representative whole-heart BOLD response from a dog under a single hypercapnic/normocapnic stimulation using the new imaging sequence. A midventricular BOLD response from the same animal acquired under similar conditions, using the standard short breath-held 2D BOLD-CMR, is shown for reference. The myocardial BOLD responses from the 2D and 3D approaches were similar, albeit both approaches showed marked heterogeneity of response. Figure 3D shows the statistical framework we used to identify the healthy myocardial territories, which required subjecting the study participants to repeat hypercapnic/normocapnic stimulations. The whole-heart T_2 images at each state of $PaCO_2$ acquired under hypercapnic/normocapnic conditions were registered to the initial 3D myocardial T_2 maps acquired under normocapnia using nonrigid registration [Advanced Normalization Tools (ANTs)] (*24*). Subsequently, animals underwent repeat hypercapnic/normocapnic stimulations. The whole-heart images were segmented according to the recommendation of AHA. Segmental myocardial T_2 values acquired under normocapnia and hypercapnia were compared using all the segments (hypercapnia and normocapnia pair) with ANOVA statistics to test the null hypothesis:

H_0 [Null: BOLD response absent]: T_2 during normocapnia = T_2 during hypercapnia.

H_1 [Alternate: BOLD response present]: T_2 during normocapnia ≠ T_2 during hypercapnia.

Null hypotheses were rejected when $P < 0.05$. The segmental *P* values from repeated-measures one-way ANOVA were used to create SPMs as shown in Fig. 3D. In these maps, myocardial segments with $P < 0.05$ were the segments showing statistically significant BOLD response to hypercapnia after one or more hypercapnic stimulations.

Using this approach, we studied healthy dogs exposed to intermittent hypercapnia, mapping segmental *P* values as SPM after each stimulation (Fig. 4A). Although there was marked heterogeneity in BOLD response after a single stimulation, the statistical confidence in observing a BOLD response increased with each repeat stimulation and became homogeneous across the heart. Direct comparison between results averaged across all AHA segments as a function of number of stimulations, along with ^{13}N-ammonia PET map of myocardial perfusion reserve (MPR), demonstrated that the mean and SD of the *P* values observed after each stimulation derived across all myocardial segments of the heart decreased with each repeat stimulation (Fig. 4B). The MPR derived from PET images under hypercapnia and normocapnia in the same animal and imaging session confirmed the absence of perfusion deficits and uniform vasodilatory response across the left ventricle (Fig. 4B). After a single stimulation, there was marked heterogeneity in *P* values suggesting that healthy myocardium can be mischaracterized as nonresponsive, likely because of dominance of noise over small BOLD signal change (Fig. 4C); however, with repeat stimulation, the noise and thus the errors were markedly reduced. These results support the notion that when repeat hypercapnic stimulations are combined with confounder-corrected fast 3D BOLD-CMR, it is possible to substantially increase the confidence in detecting healthy myocardial territories without contrast agent or ionizing radiation to extents that are realized with the gold standard, ^{13}N-ammonia PET.

Repeat hypercapnia and whole-heart BOLD-CMR for determining the myocardium at risk

Having demonstrated that BOLD response can be accurately detected in healthy myocardium using an approach that integrates the results from repeat hypercapnic stimulation to generate SPMs, we tested whether this approach could be used to identify myocardial territories affected by a functionally important coronary stenosis (reversible perfusion defect territories). We performed additional studies in the same dogs ($n = 7$) that underwent 3D acquisitions in the absence of coronary stenosis, using non–flow-limiting LAD coronary stenosis and repeat stimulations. Whole-heart BOLD images were acquired at each of the hypercapnic and normocapnic states for a total of four blocks (each block consisting of hypercapnia and normocapnia, similar to Fig. 3A). As before, hearts were registered using ANTs (*24*), the myocardium was segmented according to the AHA recommendation, and statistical framework was applied using the same hypothesis tests to identify remote (unaffected/healthy) myocardial territories. The *P* values were then used to construct SPMs of the heart.

We observed marked heterogeneity in BOLD response throughout the myocardium after single stimulation; the two myocardial territories converged with increasing number of stimulations (Fig. 5A).

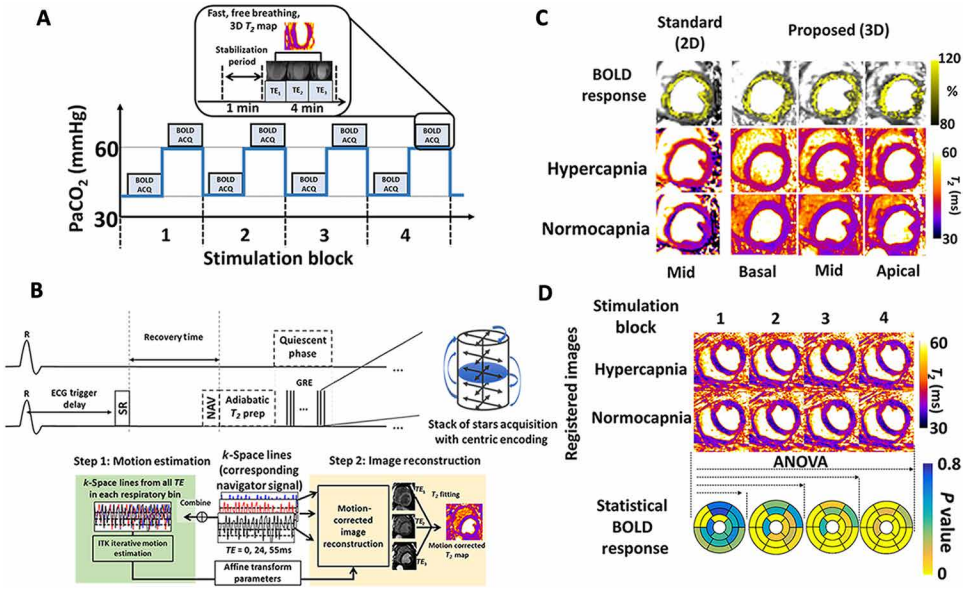

Fig. 3. Cardiac fMRI framework integrating MRI, hypercapnic stimulation, and statistical analysis. (**A**) Data acquisition framework: The approach used to acquire 3D MRI under periodic changes in $PaCO_2$ (normocapnic and hypercapnic conditions), preceded by a short delay (stabilization period) to ensure that the acquisitions are only triggered once the desired $PaCO_2$ values are reached. Acq, acquisition. (**B**) Time-efficient, free-breathing, confounder-corrected whole-heart T_2 mapping. Left: The timing diagram shows a T_2 preparation scheme composed of composite adiabatic RF pulses and spoiled GRE readout, used to minimize B_1 and B_0 artifacts at 3 T. An SR preparation was added to eliminate the signal dependence on heart rate between segmented readouts, and navigator (NAV) pulses were added to monitor the respiratory motion during acquisition. Right: The centric-encoding scheme with hybrid trajectory to ensure optimal T_2 weighting. Bottom: motion-correction algorithm and T_2 mapping. Respiratory motion was corrected using a previously described algorithm (*36*). The details of the pulse sequence development are provided in the "MRI pulse sequence development" section in the Supplementary Materials. (**C**) 3D myocardial BOLD response: 3D T_2 maps (basal, midventricular, and apical) acquired during normocapnia and hypercapnia (single stimulation block). For reference, results from 2D imaging obtained from a midventricular slice are also shown (left column). BOLD response was computed as ((hypercapnic myocardial T_2)/(normocapnia myocardial T_2)) × 100%. (**D**) Statistical framework: A schematic of the statistical framework using repeated-measures one-way ANOVA to discriminate between registered images of myocardial segments that are or are not statistically responsive, based on the hypothesis testing outlined in text, after each repeat hypercapnic/normocapnic stimulation. The polar maps on the lower row show the AHA segmentation with *P* values assigned on the statistical test.

The spatial localization of these territories was visually concordant with the ^{13}N-ammonia PET MPR (Fig. 5B) after repeat stimulation. The segmental territories identified as "remote" and "affected" based on ^{13}N-ammonia PET MPR showed distinct statistical characteristics. For the case in Fig. 5A, the mean and SD of the *P* values of all remote territories were significantly lower than those of the affected territories independent of the number of stimulations. The *P* values of the remote territories quickly converged to low values after the second hypercapnic stimulation and reached statistical significance by the fourth hypercapnic stimulation. However, the affected territories retained high *P* values and were heterogeneous despite the increasing number of stimulations. These observations were consistent with the observed spatial differences in MPR based on ^{13}N-ammonia PET and were consistent across all animals (Fig. 5C). We found that nearly all measurements showed a sensitivity >80% in identifying the affected myocardium, regardless of the number of stimulations. However, the specificity for identifying healthy myocardium was only 36% with a single stimulation. The specificity increased significantly with each additional stimulation, reaching 92% after the fourth stimulation. A similar observation was evident with accuracy; whereas the accuracy after a single stimulation was 49%, the accuracy increased substantially with each increasing stimulation and reached 91% after the fourth stimulation. These results support the notion that an SPM approach, which is enabled by repeatedly stimulating the heart with prospective control of the $PaCO_2$ and fast, 3D whole-heart T_2 mapping, can markedly increase the accuracy of BOLD-CMR for identifying hypoperfused, at-risk, myocardial territories to levels observed with ^{13}N-ammonia PET.

DISCUSSION

Accurate identification of at-risk myocardial territories affected by coronary artery disease is critical for managing patients with IHD. Current methods used for this purpose, however, require ionizing radiation or exogenous contrast media. In the best case, these methods expose patients to incremental risk; in the worst case, they are contraindicated. Previous efforts to address these limitations by using myocardial BOLD-CMR have made important progress; however, clinical adoption remains uncertain because of limited reliability. Here, we demonstrated how to overcome this key obstacle using an approach that identifies the affected and healthy/remote myocardial territories using a statistical framework. This method uses intermittent hypercapnia to repeatedly stimulate MBF combined with rapid, free-breathing whole-heart T_2 mapping to acquire BOLD images and a computational platform to perform motion-corrected registration and segmentation.

Using a clinically relevant animal model, we demonstrated that repeat modulation of MBF changes in the heart with hypercapnia and 2D T_2 CMR with limited spatial coverage (single, short-axis slice) can be used to identify healthy myocardium in animals without coronary stenosis and affected and remote myocardial segments in animals with coronary stenosis. To overcome the spatial coverage and registration limitations inherent to the 2D approach, we developed a time-efficient, confounder-corrected, whole-heart T_2 mapping that can be performed under free-breathing conditions. We then applied this imaging approach with rapid prospective control of $PaCO_2$ to generate whole-heart myocardial BOLD images under hypercapnia and normocapnia. These datasets were coregistered and analyzed segmentally in a statistical framework to demonstrate that SPMs can be generated to accurately identify the healthy myocardium in animals without coronary narrowing. Last, we extended the approach in animals with controlled coronary artery stenosis to objectively identify healthy and affected myocardium in the setting of clinically important coronary stenosis with >90% sensitivity, specificity, and accuracy.

Our study assessed segmental changes in myocardial perfusion based on the changes in myocardial oxygenation associated with clinically important coronary stenosis. Although sufficient to meet the current clinical need in the setting of coronary artery disease, expanding this approach to pixel-wise assessment of myocardial oxygenation would enable testing of novel physiological hypotheses related to IHD. For instance, pixel-wise cfMRI could be used to evaluate alterations in microcirculatory oxygenation, which could empower the assessment of microvascular disease in which MBF to the subendocardium is believed to be impaired, even in the absence of occlusive coronary disease. Current methods do not have the capacity to confirm or refute this hypothesis because available imaging methods rely on washout kinetics of contrast medium rather than oxygenation. Hence, pixel-wise assessment of myocardial oxygenation enabled by cfMRI could be instrumental in accurately discerning whether the transmural changes in blood flow and oxygenation occur in parallel. Such an understanding could provide new insights into mechanisms of angina development in patients with microvascular disease and could help evaluate therapies to alleviate microvascular impairments in oxygenation. Studies of this nature are likely to demand more advanced segmentation and registration approaches so that pixel-wise analysis can be accurately performed. We anticipate that these demands can be met with innovative segmentation and registration algorithms that are actively being developed for cardiac image analysis (*25*). In addition, to enable pixel-wise SPM, additional studies would be required to determine the number of minimum stimulations necessary for accurate assessment of BOLD signal changes at the pixel level.

There are multiple other conditions for which cfMRI could be useful. cfMRI identifies the affected regions of the myocardium that do not respond to repeat hypercapnic stimulation. Although we used this approach to identify territories affected by stenosis of a single coronary vessel, we anticipate that this approach can be applied to other patterns of coronary artery disease, such as identifying clinically important multivessel coronary artery disease. In addition, cfMRI may also be used to examine changes in myocardial oxygenation of nonischemic origin, such as hypertrophic heart disease, which is known to impair myocardial oxygenation reserve (*13*). Although our studies showed that cfMRI can identify substantially reduced blood

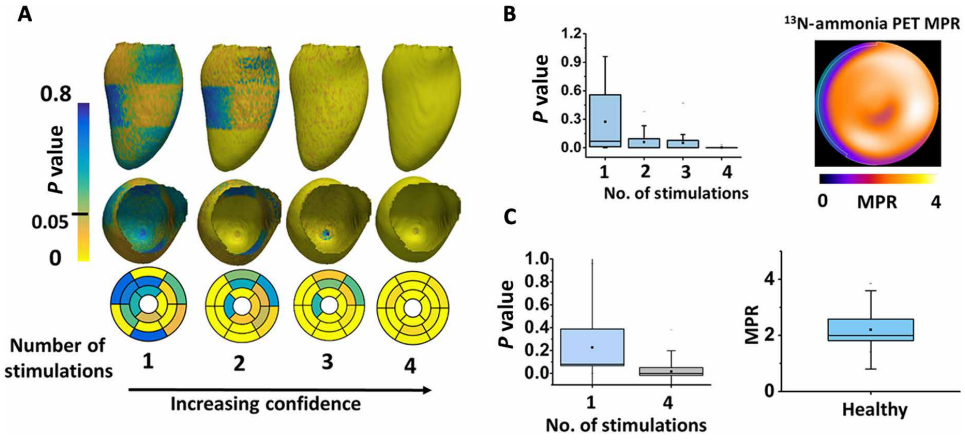

Fig. 4. Application of cardiac fMRI approach for reliable identification of healthy myocardium. (**A**) Myocardial statistical parametric mapping (SPM). Long- and short-axis volume rendered views of the heart with intensities denoting segmental *P* values derived from the statistical framework from a typical healthy dog. Bottom: polar maps of *P* values. (**B**) Myocardial SPM versus ^{13}N-ammonia PET in a representative case. The graph (left) shows the mean and SD of *P* values across all segments for the case in (A) as a function of number of stimulation blocks (one through four). The image (right) shows the corresponding ^{13}N-ammonia PET MPR. (**C**) Myocardial SPM versus ^{13}N-ammonia PET MPR. Graphs show the average *P* values across all dogs ($n = 8$) and all myocardial segments after one and four stimulations (left) and the mean and scatter of MPR across all animals in response to hypercapnia (right). *P* values were derived from repeated-measures one-way ANOVA and $P < 0.05$ was used for statistical significance.

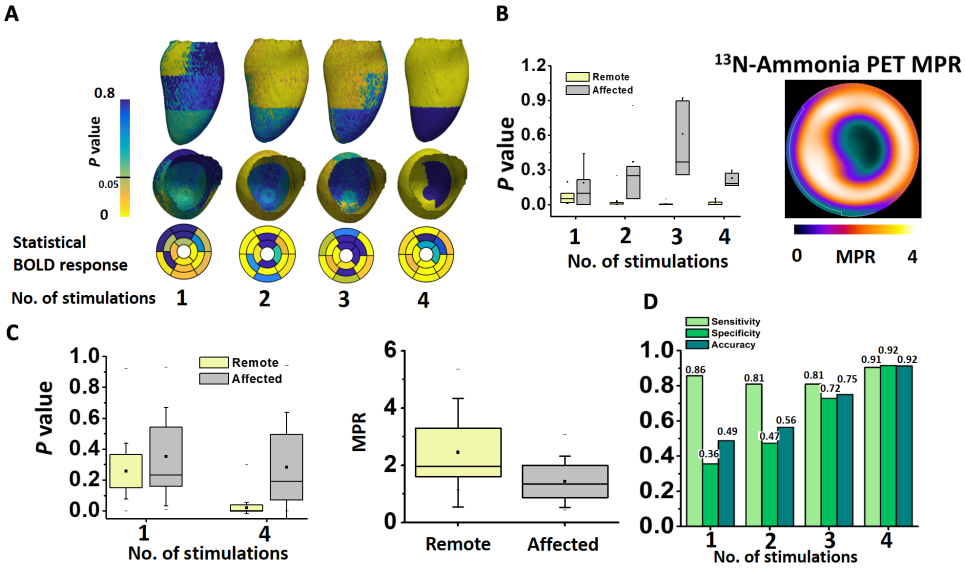

Fig. 5. Cardiac fMRI-based SPM for identification of myocardial segments affected by clinically relevant coronary stenosis. (**A**) Myocardial SPM under coronary stenosis. Representative images of long- and short-axis volume rendered views of the heart with intensities denoting segmental *P* values derived from the statistical framework from one dog with clinically important coronary stenosis. Bottom: polar maps of *P* values for the AHA segments. (**B**) Myocardial SPM versus ^{13}N-ammonia PET for a representative case. Left: mean and SD of *P* values across affected and remote segments for the case in (A) as a function of number of stimulation blocks (one through four). Right: the corresponding ^{13}N-ammonia PET MPR. (**C**) Myocardial SPM versus ^{13}N-ammonia PET MPR for all cases (dogs, $n = 7$). Left: average response across all animals in the affected and remote myocardial segments after one and four stimulations. Right: mean and scatter of PET MPR across all animals in the remote and affected segments after hypercapnia. (**D**) Sensitivity, specificity, and accuracy determined after each stimulation with PET serving as the ground truth. *P* values were derived from repeated-measures one-way ANOVA and $P < 0.05$ was used for statistical significance.

flow and oxygenation, identification of early changes in myocardial oxygenation (from subclinical coronary stenosis or early changes in the heart due to hypertrophy) would require additional studies. We anticipate that these studies would benefit from refined statistical hypotheses and/or selection of optimal statistical thresholds that build on identifying myocardial territories of interest based on cfMRI.

Given the lack of invasive or noninvasive methods to directly assess myocardial oxygenation in vivo, we demonstrated the capacity of cfMRI to accurately identify myocardial territories affected by coronary stenosis, using ^{13}N-ammonia PET under identical physiological conditions. Nonetheless, the tapering off in sensitivity and specificity between cfMRI and ^{13}N-ammonia PET at ~90% may suggest potential differences between flow and oxygenation. Further studies would be needed to probe the conditions under which myocardial oxygenation and flow changes are congruent or different.

Other methods to assess IHD without contrast agents or ionizing radiation are under development or are emerging (*10*, *26*). Among these, spectroscopic CMR approaches have the capacity to offer insight into myocardial oxygenation, but they have not been successfully translated into clinical practice because of poor reliability (*27*). In addition, a recent study using native T_1 CMR has successfully demonstrated that IHD can be identified without exogenous contrast agents or ionizing radiation (*10*). Although this approach appears promising, randomized multicenter studies to evaluate the capacity of native T_1 CMR for diagnosis of IHD in spectrum of patients presenting with the disease are necessary before its widespread adoption.

The proposed method builds on previous studies from our laboratory and elsewhere, which showed that tolerable amounts of hypercapnia led to more than twofold increases in MBF and modulation in oxygenation similar in extent to that observed with adenosine (a commonly used coronary vasodilator) both in dogs and in humans (*22*, *28*). Although our findings in this study are limited to dogs, given that all cardiac stress testing paradigms have been first successfully demonstrated in dogs, and a 25-mmHg increase in $PaCO_2$ is tolerable in humans, we anticipate that the proposed approach would translate well in humans. To date, hypercapnia has been shown to be safe and tolerable in a broad spectrum of patients (age range, 9 to 88 years) (*29*). Furthermore, hypercapnic stimulus in conjunction with imaging has been extensively studied in patients with neurovascular disease (*29*). Accordingly, there is precedence for using hypercapnia in patients.

Given the growing availability of MRI systems, the infrastructure costs required to translate the proposed approach into the clinical settings, which already have access to MRI suites, is expected to be minimal (costing less than 1% of the total cost of the scanner environment). Furthermore, since the proposed strategy does not require contrast agents or infusion pumps, it would yield substantial cost savings to the medical centers relative to the status quo. Although a direct translation of the proposed approach in the current state is expected to take ~40 min in human subjects, compared to the ~10 to 15 min of imaging duration with standard methods, methods that can reduce scan time (for example, through faster data acquisitions taking advantage of spatiotemporal redundancies in conjunction with use of generalized linear models for signal analysis) are expected to permit the proposed approach to be executed within the standard duration of cardiac stress tests. This would also limit the hypercapnic durations to a much shorter time (<4 min).

Although a 25-mmHg increase in $PaCO_2$ is expected to be tolerable by most people, some may find it uncomfortable, which may be addressed by taking advantage of the flexibility cfMRI offers for fine-tuning image acquisition and analysis. For example, in patients who could tolerate only a lower hypercapnic stimulus, a greater number of weaker hypercapnic stimulations may offer a viable alternative. When this is combined with accelerated data acquisition strategies to yield images of higher temporal resolution to deploy advanced statistical methods that automatically find thresholds of affected regions in a multivariate fashion, it may be possible to identify myocardial territories supplied by stenotic coronary arteries, even in patients with lower tolerance for hypercapnia (*30*). Alternatively, in patients who can tolerate 25 mmHg of stimulus but cannot tolerate multiple repeat stimulations of it, an alternative may be rapid acquisition of images under other waveforms of $PaCO_2$ (for example, ramps instead of blocks or shorter frequency with longer duration of hypercapnia), which are all possible with the proposed prospective control of $PaCO_2$.

Although the proposed approach has notable strengths, it is not without limitations. First, unlike the existing methods that use pharmacological stress, contrast media, and/or ionizing radiation, cfMRI requires a gas controlling system, which is an additional expense and one that may require a skilled operator for gas control—albeit this individual may be no different from one who is typically present during standard pharmacological stress tests, such as a nurse practitioner. Moreover, given that the proposed approach relies on $PaCO_2$ to alter the vasodilatory capacity of the coronaries, the capability of the approach in individuals with respiratory disorders (asthma, chronic pulmonary disorder) in whom IHD is suspected is unclear and requires careful investigation. Last, the proposed approach requires a clinical MRI system with high-performance hardware and software, which is not always within reach for everyone, although it is becoming common.

Despite these limitations, the proposed approach may open the door to new opportunities for cardiac stress testing in some of the most vulnerable patients. First, cardiac stress testing may be enabled in adult patients with renal insufficiency, who would otherwise receive multiple doses of ionizing radiation, which can expose them to greater risks associated with radiation. It also offers an alternative to patients who are not candidates for exercise or intravenously administered vasodilatory agents as part of stress tests. Furthermore, it may enable cardiac stress testing in the children without ionizing radiation, contrast agents, pharmacological stress, or needles. Accordingly, there is substantial motivation to translate the proposed approach not only to incrementally improve existing care but also to enable management of IHD in those who are contraindicated for standard cardiac stress tests.

cfMRI enables noninvasive determination of healthy myocardium and myocardium affected by reversible perfusion defects due to coronary stenosis based on myocardial oxygenation. This integrated approach has the capacity to open a new paradigm for a radiation-, contrast-, and needle-free approach for accurately determining reversible perfusion defects in patients suspected of having functionally important coronary artery disease. Furthermore, it has the desirable characteristics to access multiple other myocardial pathologies on the basis of oxygenation.

MATERIALS AND METHODS

Study design

The objective of this study was to develop a needle-free BOLD-CMR approach for detecting myocardial ischemic territories without

exogenous contrast agents, intravenously administered pharmacological stress agents, and radiation. This was studied in two parts. In the first set, experiments were performed in dogs with (n = 5) and without (n = 5) controlled coronary stenosis under repeat hypercapnic stimulus using free-breathing 2D BOLD-CMR to evaluate whether the repeat stimulations can improve the visualization and contrast-to-noise ratio between normal and ischemic territories. In the second set of experiments, a time-efficient, confounder-corrected, 3D cardiac BOLD-CMR sequence was developed to enable whole-heart evaluation of myocardial oxygenation changes. This approach was tested in dogs with (n = 7) and without (n = 8) coronary artery stenosis. Subsequently, a statistical model–based approach was used to derive the statistical significance of the myocardial BOLD response, and the findings were validated against simultaneously acquired ^{13}N-ammonia PET. The details regarding modulation of $PaCO_2$, imaging protocol (both MRI and ^{13}N-ammonia PET), the development of 3D BOLD-CMR approach, image analysis (segmentation and registration) and statistical modeling of BOLD-CMR response, and statistical analysis are described in the "Statistical analysis" section; an overview schematic is provided in fig. S1. Individual subject-level data are provided in data file S1.

Animal preparation and method for inducing coronary stenosis

Dogs (n = 15, 20 to 25 kg) were studied with and without surgically induced coronary stenosis. All animals were studied according to the National Institutes of Health (NIH) *Guide for the Care and Use of Laboratory Animals* following approval of the Institutional Animal Care and Use Committee. In a subset of the animals, a left lateral thoracotomy was performed as previously described by our group (*22*). A Doppler probe was attached distal to the first branch of the LAD to enable measurement of coronary blood flow velocity. An externally actuated hydraulic occluder was affixed proximal to the Doppler flow probe. Subsequently, the chest was closed, and the animals were allowed to recover for at least 7 days before imaging studies. Before all imaging studies, animals were fasted, sedated, intubated, and anesthetized. During the imaging studies, anesthesia was maintained with a continuous infusion of propofol. Dogs were transferred to the PET/MR scanner table and were mechanically ventilated through the RespirAct (Thornhill Research Inc.) with parameters reported in previous studies (*23*). In stenosis studies, coronary stenosis was induced before commencing imaging. The perfusion level during rest and stress was confirmed with ^{13}N-ammonia PET images. Before or immediately after the baseline ($PETCO_2$ = 35 mmHg) and peak hypercapnia ($PETCO_2$ = 60 mmHg) BOLD acquisitions, the Doppler transducer (Triton Technologies Inc.) was connected to the wires originating from the surgically implanted Doppler probe and root mean square Doppler flow velocity values were recorded. In dogs where LAD stenosis was to be induced, peak hyperemic coronary blood flow velocity measured at $PETCO_2$ = 60 mmHg was reduced to coronary blood flow velocity measured at $PETCO_2$ = 35 mmHg to provide a standardized hemodynamically effective constriction that does not decrease blood flow below baseline flow under resting conditions (normocapnia).

Modulation of arterial pressure of CO_2

Prospective targeting of PaO_2 and $PaCO_2$ was implemented using a validated gas controlling system (RespirAct). The principles of controlling end-tidal gases have been previously described (*31*). In this study, we targeted hypercapnia at $PaCO_2$ = 60 mmHg with PaO_2 = 130 mmHg and normocapnia at $PaCO_2$ = 35 mmHg with PaO_2 = 130 mmHg. These targets were synchronized with CMR and PET acquisitions. Before each image acquisition, $PaCO_2$ were stabilized at the targeted concentration for 1 min to ensure that target $PaCO_2$ values were reached. Physiologic response to the stimulations is summarized in table S1.

Imaging protocol

In all imaging studies, ^{13}N-ammonia PET and BOLD-CMR images were simultaneously acquired using a clinical PET/MR scanner. In animals without coronary stenosis, PET images were acquired under rest and hypercapnia (6 min) to quantify the MBF under different physiological conditions. A time delay was introduced between sequential PET acquisitions at each physiological condition to ensure sufficient decay of each ^{13}N-ammonia dose (five half-lives, ~50 min). After the first PET scan, four sets of prospectively targeted normocapnia and hypercapnia stimulations were induced using RespirAct. The $PaCO_2$ concentrations were maintained for 5 min during each physiological state (fig. S2). BOLD-CMR images were acquired 1 min after reaching the targeted $PETCO_2$ concentration. In animals with coronary stenosis, baseline blood flow before surgery was compared to baseline flow after surgery (on the day of stenosis studies) using ^{13}N-ammonia PET. LAD coronary stenoses were induced before the first PET acquisition. Other aspects of the imaging protocol were similar to that implemented in intact animals. A schematic representation of the time course of execution of the study protocol is shown in fig. S2. During repeat stimulations, two BOLD acquisition methods (2D and 3D T_2 maps) were used in a subgroup of animals. In 2D studies (n = 5 for both intact and stenosis groups), a conventional 2D T_2 mapping sequence was prescribed over a midventricular slice. Images were acquired under short breath holds (<10 s) at 2 and 5 min after target $PETCO_2$ values were reached. In the 3D acquisitions, the proposed 3D sequence was prescribed under free-breathing conditions starting 1 min after the targeted $PETCO_2$ concentration was reached.

MRI pulse sequence development

A heart rate–independent, free-breathing, 3D T_2 mapping prototype sequence with whole-heart left ventricular coverage, which minimizes the sensitivity to B_0 and B_1 field inhomogeneities, was developed for the PET/MR system. Adiabatic T_2 preparation with spoiled gradient-echo (GRE) readout was used to minimize B_0 and B_1 artifacts that are otherwise prominent at 3 T and confound BOLD signal readouts. To improve imaging efficiency and enable data acquisition under free-breathing conditions, a motion-correction platform with a hybrid Cartesian-radial trajectory was applied that permits near-perfect imaging efficiency. To further increase acquisition speed and minimize the signal dependence on heart rate between rest and stress, a saturation recovery (SR) preparation was integrated with a constant saturation recovery time (T_{SR}) to reset longitudinal magnetization in every heartbeat (*32*–*34*). To minimize any potential confounding effects associated with differences in T_1 recovery after T_2 preparation under rest and stress (*10*), data were collected and centrically encoded in the through-plane direction. Images were acquired with three incremental T_2 preparation times [echo time (TE) = 0, 24, and 55 ms], and T_2 maps were reconstructed using a custom-written MATLAB (MathWorks) script. The accuracy of the proposed approach was studied with computer simulations and ex vivo tissue preparations (fig. S3).

Assessment of MBF with simultaneously acquired ^{13}N PET

All PET images were acquired in 3D list mode using ^{13}N-ammonia [100 MBq, IV bolus (30 s) followed by 10 cm^3 saline flush] as the blood flow tracer. Before each PET scan, MR images were acquired to correct for photon attenuation. A two-point Dixon MRI imaging pulse sequence was used for segmentation and attenuation correction. PET data were acquired over 10 min and were started a few seconds before the ^{13}N-ammonia injection. In animals without coronary stenosis, images were acquired during hypercapnia and at normocapnia to determine the MBF response in the absence of coronary stenosis. In animals with coronary stenosis, images were acquired at rest and during hypercapnia after infliction of LAD stenosis. The MRI attenuation map and PET images were aligned and adjusted by an experienced technologist. Dynamic PET images were reconstructed with different time periods (twelve 10-s, two 30-s, one 1-min, and one 6-min frames, for a total of 10 min). Images were reconstructed with three iterations and 3D post-filtering with a 5-mm Gaussian kernel. Data were reconstructed with 2-mm pixels for each dynamic frame. MBF (ml min^{-1} g^{-1}) was derived from the PET data using the automated QPET software (Cedars-Sinai Medical Center), as shown previously (*35*).

Statistical analysis

Simulations: Statistical modeling of myocardial BOLD response

Rest BOLD signals were generated for each segment with Gaussian distribution with the mean (μ) and SD (δ) reported in previous studies acquired using cardiac 2D T_2 mapping (*34*, *36*). Stress signals were generated randomly on the basis of the rest signal and BOLD response [μStress signal = μRest signal + μBOLD response (1 to 20%)] and the number of repeat measurements (1 to 30). BOLD signals from each segment were grouped into rest and stress states and compared using repeated-measures ANOVA that tested the following hypotheses:

H_0 [Null: BOLD response absent]: T_2 during normocapnia = T_2 during hypercapnia.

H_1 [Alternate: BOLD response present]: T_2 during normocapnia ≠ T_2 during hypercapnia.

Each test was repeated 200 times and averaged P values were reported for each peak BOLD response and number of measurements. Sequential Holm-Bonferroni corrections were used to adjust for multiple measurements.

Statistical image analysis

The BOLD images acquired under different physiological states were first segmented according to the AHA 16-segment model (*37*) and were used as multiple samples to test the null hypothesis described in the previous section. Repeated-measures ANOVA tests were used to compare cumulative BOLD signals from each segmental position for increasing stimulation pairs 1 to 4. Sequential Holm-Bonferroni corrections were used to adjust for multiple measurements. Significance was set at $\alpha = 0.05$.

SUPPLEMENTARY MATERIALS

stm.sciencemag.org/cgi/content/full/11/494/eaat4407/DC1

Materials and Methods

Fig. S1. Schematic of the cardiac fMRI approach.

Fig. S2. Imaging study protocol.

Fig. S3. Computer simulations and ex vivo experiments.

Table S1. Physiological parameters during normocapnia and hypercapnia.

Data file S1. Individual subject-level data.

References (*38*, *39*)

REFERENCES AND NOTES

1. Writing Group Members, D. Lloyd-Jones, R. J. Adams, T. M. Brown, M. Carnethon, S. Dai, G. De Simone, T. B. Ferguson, E. Ford, K. Furie, C. Gillespie, A. Go, K. Greenlund, N. Haase, S. Hailpern, P. M. Ho, V. Howard, B. Kissela, S. Kittner, D. Lackland, L. Lisabeth, A. Marelli, M. M. McDermott, J. Meigs, D. Mozaffarian, M. Mussolino, G. Nichol, V. L. Roger, W. Rosamond, R. Sacco, P. Sorlie, V. L. Roger, T. Thom, S. Wasserthiel-Smoller, N. D. Wong, J. Wylie-Rosett, American Heart Association Statistics Committee and Stroke Statistics Subcommittee, Heart disease and stroke statistics—2010 update: A report from the American Heart Association. *Circulation* **121**, e46–e215 (2010).
2. N. G. Uren, J. A. Melin, B. De Bruyne, W. Wijns, T. Baudhuin, P. G. Camici, Relation between myocardial blood flow and the severity of coronary-artery stenosis. *N. Engl. J. Med.* **330**, 1782–1788 (1994).
3. L. J. Shaw, D. S. Berman, D. J. Maron, G. B. Mancini, S. W. Hayes, P. M. Hartigan, W. S. Weintraub, R. A. O'Rourke, M. Dada, J. A. Spertus, B. R. Chaitman, J. Friedman, P. Slomka, G. V. Heller, G. Germano, G. Gosselin, P. Berger, W. J. Kostuk, R. G. Schwartz, M. Knudtson, E. Veledar, E. R. Bates, B. McCallister, K. K. Teo, W. E. Boden, COURAGE Investigators, Optimal medical therapy with or without percutaneous coronary intervention to reduce ischemic burden: Results from the Clinical Outcomes Utilizing Revascularization and Aggressive Drug Evaluation (COURAGE) trial nuclear substudy. *Circulation* **117**, 1283–1291 (2008).
4. W. S. Weintraub, J. A. Spertus, P. Kolm, D. J. Maron, Z. Zhang, C. Jurkovitz, W. Zhang, P. M. Hartigan, C. Lewis, E. Veledar, J. Bowen, S. B. Dunbar, C. Deaton, S. Kaufman, R. A. O'Rourke, R. Goeree, P. G. Barnett, K. K. Teo, W. E. Boden, COURAGE Trial Research Group, G. B. Mancini, Effect of PCI on quality of life in patients with stable coronary disease. *N. Engl. J. Med.* **359**, 677–687 (2008).
5. BARI 2D Study Group, R. L. Frye, P. August, M. M. Brooks, R. M. Hardison, S. F. Kelsey, J. M. MacGregor, T. J. Orchard, B. R. Chaitman, S. M. Genuth, S. H. Goldberg, M. A. Hlatky, T. L. Jones, M. E. Molitch, R. W. Nesto, E. Y. Sako, B. E. Sobel, A randomized trial of therapies for type 2 diabetes and coronary artery disease. *N. Engl. J. Med.* **360**, 2503–2515 (2009).
6. R. J. Gibbons, G. J. Balady, J. T. Bricker, B. R. Chaitman, G. F. Fletcher, V. F. Froelicher, D. B. Mark, B. D. McCallister, A. N. Mooss, M. G. O'Reilly, W. L. Winters Jr., R. J. Gibbons, E. M. Antman, J. S. Alpert, D. P. Faxon, V. Fuster, G. Gregoratos, L. F. Hiratzka, A. K. Jacobs, R. O. Russell, S. C. Smith Jr., American College of Cardiology/American Heart Association Task Force on Practice Guidelines (Committee to Update the 1997 Exercise Testing Guidelines), ACC/AHA 2002 guideline update for exercise testing: Summary article: A report of the American College of Cardiology/American Heart Association Task Force on Practice Guidelines (Committee to Update the 1997 Exercise Testing Guidelines). *Circulation* **106**, 1883–1892 (2002).
7. Multimodality Writing Group for Stable Ischemic Heart Disease, M. J. Wolk, S. R. Bailey, J. U. Doherty, P. S. Douglas, R. C. Hendel, C. M. Kramer, J. K. Min, M. R. Patel, L. Rosenbaum, L. J. Shaw, R. F. Stainback, J. M. Allen, Panel Technical, R. G. Brindis, C. M. Kramer, L. J. Shaw, M. D. Cerqueira, J. Chen, L. S. Dean, R. Fazel, W. G. Hundley, D. Itchhaporia, P. Kligfield, R. Lockwood, J. E. Marine, R. B. McCully, J. V. Messer, P. T. O'Gara, R. J. Shemin, L. S. Wann, J. B. Wong, Appropriate Use Criteria Task Force, M. R. Patel, C. M. Kramer, S. R. Bailey, A. S. Brown, J. U. Doherty, P. S. Douglas, R. C. Hendel, B. D. Lindsay, J. K. Min, L. J. Shaw, R. F. Stainback, L. S. Wann, M. J. Wolk, J. M. Allen, ACCF/AHA/ASE/ASNC/HFSA/HRS/SCAI/SCCT/SCMR/STS 2013 multimodality appropriate use criteria for the detection and risk assessment of stable ischemic heart disease: A report of the American College of Cardiology Foundation Appropriate Use Criteria Task Force, American Heart Association, American Society of Echocardiography, American Society of Nuclear Cardiology, Heart Failure Society of America, Heart Rhythm Society, Society for Cardiovascular Angiography and Interventions, Society of Cardiovascular Computed Tomography, Society for Cardiovascular Magnetic Resonance, and Society of Thoracic Surgeons. *J. Card. Fail.* **20**, 65–90 (2014).
8. A. Berrington de Gonzalez, K.-P. Kim, R. Smith-Bindman, D. McAreavey, Myocardial perfusion scans: Projected population cancer risks from current levels of use in the United States. *Circulation* **122**, 2403–2410 (2010).
9. W. A. High, R. A. Ayers, J. Chandler, G. Zito, S. E. Cowper, Gadolinium is detectable within the tissue of patients with nephrogenic systemic fibrosis. *J. Am. Acad. Dermatol.* **56**, 21–26 (2007).
10. A. Liu, R. S. Wijesurendra, J. M. Francis, M. D. Robson, S. Neubauer, S. K. Piechnik, V. M. Ferreira, Adenosine stress and rest T1 mapping can differentiate between ischemic, infarcted, remote, and normal myocardium without the need for gadolinium contrast agents. *JACC Cardiovasc. Imaging* **9**, 27–36 (2016).
11. M. G. Friedrich, T. D. Karamitsos, Oxygenation-sensitive cardiovascular magnetic resonance. *J. Cardiovasc. Magn. Reson.* **15**, 43 (2013).
12. T. D. Karamitsos, L. Leccisotti, J. R. Arnold, A. Recio-Mayoral, P. Bhamra-Ariza, R. K. Howells, N. Searle, M. D. Robson, O. E. Rimoldi, P. G. Camici, S. Neubauer, J. B. Selvanayagam, Relationship between regional myocardial oxygenation and perfusion in patients with coronary artery disease: Insights from cardiovascular magnetic resonance and positron emission tomography. *Circ. Cardiovasc. Imaging* **3**, 32–40 (2010).

13. T. D. Karamitsos, S. Dass, J. Suttie, E. Sever, J. Birks, C. J. Holloway, M. D. Robson, M. Jerosch-Herold, H. Watkins, S. Neubauer, Blunted myocardial oxygenation response during vasodilator stress in patients with hypertrophic cardiomyopathy. *J. Am. Coll. Cardiol.* **61**, 1169–1176 (2013).
14. R. Dharmakumar, D. Li, *Cardiovascular Magnetic Resonance*, W. Manning, D. Pennell, Eds (Saunders, Elsevier, 2010), pp. 569–579.
15. M. K. Atalay, J. R. Forder, V. P. Chacko, S. Kawamoto, E. A. Zerhouni, Oxygenation in the rabbit myocardium: Assessment with susceptibility-dependent MR imaging. *Radiology* **189**, 759–764 (1993).
16. D. Li, P. Dhawale, P. J. Rubin, E. M. Haacke, R. J. Gropler, Myocardial signal response to dipyridamole and dobutamine: Demonstration of the BOLD effect using a double-echo gradient-echo sequence. *Magn. Reson. Med.* **36**, 16–20 (1996).
17. M. G. Friedrich, T. Niendorf, J. Schulz-Menger, C. M. Gross, R. Dietz, Blood oxygen level-dependent magnetic resonance imaging in patients with stress-induced angina. *Circulation* **108**, 2219–2223 (2003).
18. C. Jahnke, R. Gebker, R. Manka, B. Schnackenburg, E. Fleck, I. Paetsch, Navigator-gated 3D blood oxygen level-dependent CMR at 3.0-T for detection of stress-induced myocardial ischemic reactions. *JACC Cardiovasc. Imaging* **3**, 375–384 (2010).
19. S. A. Huettel, A. W. Song, G. McCarthy, *Functional Magnetic Resonance Imaging* (Sinauer Associates, 2008).
20. S. Ogawa, T. M. Lee, A. R. Kay, D. W. Tank, Brain magnetic resonance imaging with contrast dependent on blood oxygenation. *Proc. Natl. Acad. Sci. U.S.A.* **87**, 9868–9872 (1990).
21. *FDA warns of rare but serious risk of heart attack and death with cardiac nuclear stress test drugs Lexiscan (regadenoson) and Adenoscan (adenosine)* (2013); www.fda.gov/drugs/drug-safety-and-availability/fda-warns-rare-serious-risk-heart-attack-and-death-cardiac-nuclear-stress-test-drugs-lexiscan.
22. H.-J. Yang, D. Dey, J. Sykes, M. Klein, J. Butler, M. S. Kovacs, O. Sobczyk, B. Sharif, X. Bi, A. Kali, I. Cokic, R. Tang, R. Yumul, A. H. Conte, S. A. Tsaftaris, M. Tighiouart, D. Li, P. J. Slomka, D. S. Berman, F. S. Prato, J. A. Fisher, R. Dharmakumar, Arterial CO_2 as a potent coronary vasodilator: A preclinical PET/MR validation study with implications for cardiac stress testing. *J. Nucl. Med.* **58**, 953–960 (2017).
23. H.-J. Yang, R. Yumul, R. Tang, I. Cokic, M. Klein, A. Kali, O. Sobczyk, B. Sharif, J. Tang, X. Bi, S. A. Tsaftaris, D. Li, A. H. Conte, J. A. Fisher, R. Dharmakumar, Assessment of myocardial reactivity to controlled hypercapnia with free-breathing T_2-prepared cardiac blood oxygen level-dependent MR imaging. *Radiology* **272**, 397–406 (2014).
24. B. B. Avants, N. J. Tustison, G. Song, P. A. Cook, A. Klein, J. C. Gee, A reproducible evaluation of ANTs similarity metric performance in brain image registration. *NeuroImage* **54**, 2033–2044 (2011).
25. I. Oksuz, A. Mukhopadhyay, R. Dharmakumar, S. A. Tsaftaris, Unsupervised myocardial segmentation for cardiac BOLD. *IEEE Trans. Med. Imaging* **36**, 2228–2238 (2017).
26. P. A. Bottomley, Noninvasive study of high-energy phosphate metabolism in human heart by depth-resolved 31P NMR spectroscopy. *Science* **229**, 769–772 (1985).
27. H. J. Lamb, J. Doornbos, J. A. den Hollander, P. R. Luyten, H. P. Beyerbacht, E. E. van der Wall, A. de Roos, Reproducibility of human cardiac ^{31}P-NMR spectroscopy. *NMR Biomed.* **9**, 217–227 (1996).
28. M. Pelletier-Galarneau, R. A. deKemp, C. R. R. N. Hunter, R. Klein, M. Klein, J. Ironstone, J. A. Fisher, T. D. Ruddy, Effects of hypercapnia on myocardial blood flow in healthy human subjects. *J. Nucl. Med.* **59**, 100–106 (2018).
29. V. R. Spano, D. M. Mandell, J. Poublanc, K. Sam, A. Battisti-Charbonney, O. Pucci, J. S. Han, A. P. Crawley, J. A. Fisher, D. J. Mikulis, CO_2 blood oxygen level-dependent MR mapping of cerebrovascular reserve in a clinical population: Safety, tolerability, and technical feasibility. *Radiology* **266**, 592–598 (2013).
30. M. Bevilacqua, R. Dharmakumar, S. A. Tsaftaris, Dictionary-driven ischemia detection from cardiac phase-resolved myocardial BOLD MRI at rest. *IEEE Trans. Med. Imaging* **35**, 282–293 (2016).
31. M. Slessarev, J. Han, A. Mardimae, E. Prisman, D. Preiss, G. Volgyesi, C. Ansel, J. Duffin, J. A. Fisher, Prospective targeting and control of end-tidal CO_2 and O_2 concentrations. *J. Physiol.* **581**, 1207–1219 (2007).
32. G. A. Rongen, S. C. Brooks, M. J. Pollard, S.-i. Ando, H. R. Dajani, C. F. Notarius, J. S. Floras, Effect of adenosine on heart rate variability in humans. *Clin. Sci.* **96**, 597–604 (1999).
33. H. Ding, L. Fernandez-de-Manuel, M. Schär, K. H. Schuleri, H. Halperin, L. He, M. M. Zviman, R. Beinart, D. A. Herzka, Three-dimensional whole-heart T_2 mapping at 3T. *Magn. Reson. Med.* **74**, 803–816 (2015).
34. H.-J. Yang, B. Sharif, J. Pang, A. Kali, X. Bi, I. Cokic, D. Li, R. Dharmakumar, Free-breathing, motion-corrected, highly efficient whole heart T_2 mapping at 3T with hybrid radial-cartesian trajectory. *Magn. Reson. Med.* **75**, 126–136 (2016).
35. P. J. Slomka, E. Alexanderson, R. Jácome, M. Jiménez, E. Romero, A. Meave, L. Le Meunier, M. Dalhbom, D. S. Berman, G. Germano, H. Schelbert, Comparison of clinical tools for measurements of regional stress and rest myocardial blood flow assessed with ^{13}N-ammonia PET/CT. *J. Nucl. Med.* **53**, 171–181 (2012).
36. S. Giri, Y.-C. Chung, A. Merchant, G. Mihai, S. Rajagopalan, S. V. Raman, O. P. Simonetti, T_2 quantification for improved detection of myocardial edema. *J. Cardiovasc. Magn. Reson.* **11**, 56 (2009).
37. M. D. Cerqueira, N. J. Weissman, V. Dilsizian, A. K. Jacobs, S. Kaul, W. K. Laskey, D. J. Pennell, J. A. Rumberger, T. Ryan, M. S. Verani, American Heart Association Writing Group on Myocardial Segmentation and Registration for Cardiac Imaging, Standardized myocardial segmentation and nomenclature for tomographic imaging of the heart. A statement for healthcare professionals from the Cardiac Imaging Committee of the Council on Clinical Cardiology of the American Heart Association. *Circulation* **105**, 539–542 (2002).
38. J. Fierstra, M. Machina, A. Battisti-Charbonney, J. Duffin, J. A. Fisher, L. Minkovich, End-inspiratory rebreathing reduces the end-tidal to arterial PCO_2 gradient in mechanically ventilated pigs. *Intensive Care Med.* **37**, 1543–1550 (2011).
39. R. Nakazato, D. S. Berman, D. Dey, L. Le Meunier, S. W. Hayes, J. S. Fermin, V. Y. Cheng, L. E. J. Thomson, J. D. Friedman, G. Germano, P. J. Slomka, Automated quantitative Rb-82 3D PET/CT myocardial perfusion imaging: Normal limits and correlation with invasive coronary angiography. *J. Nucl. Cardiol.* **19**, 265–276 (2012).

Acknowledgments: We thank H. Ho for the constructive discussions on the statistical elements of the study and R. Finney and L.S. Bouchard for pre-reviewing the manuscript and providing valuable suggestions for improving the manuscript. **Funding:** This work was supported in part by NIH/R01 HL091989 (R.D.), Ontario Research Fund RS7-021, Canadian Foundation for Innovation no. 11358, and education grants from Siemens Healthineers and London X-ray Associates (F.S.P.). **Author contributions**: H.-J.Y. and R.D. designed the overall study. H.-J.Y. performed the MRI technical development with the support of X.B. and D.L. H.-J.Y., M.S.K., J.S., M.K., J.B., I.C., O.S., J.A.F., and R.D. performed data acquisition. H.-J.Y., I.O., D.D., P.J.S., and M.T. analyzed the data. I.O. and S.A.T. derived the SPMs and generated the visualizations. R.D. and F.S.P. provided funding. All authors wrote and revised the manuscript. **Competing interests**: J.A.F. and O.S. are part-time employees of Thornhill Research Inc., and X.B. is an employee of Siemens Healthineers. **Data and materials availability**: All data associated with this study are present in the paper or the Supplementary Materials.

Submitted 28 February 2018
Accepted 8 May 2019
Published 29 May 2019
10.1126/scitranslmed.aat4407

Citation: H.-J. Yang, I. Oksuz, D. Dey, J. Sykes, M. Klein, J. Butler, M. S. Kovacs, O. Sobczyk, I. Cokic, P. J. Slomka, X. Bi, D. Li, M. Tighiouart, S. A. Tsaftaris, F. S. Prato, J. A. Fisher, R. Dharmakumar, Accurate needle-free assessment of myocardial oxygenation for ischemic heart disease in canines using magnetic resonance imaging. *Sci. Transl. Med.* **11**, eaat4407 (2019).

Science Translational Medicine

Accurate needle-free assessment of myocardial oxygenation for ischemic heart disease in canines using magnetic resonance imaging

Hsin-Jung Yang, Ilkay Oksuz, Damini Dey, Jane Sykes, Michael Klein, John Butler, Michael S. Kovacs, Olivia Sobczyk, Ivan Cokic, Piotr J. Slomka, Xiaoming Bi, Debiao Li, Mourad Tighiouart, Sotirios A. Tsaftaris, Frank S. Prato, Joseph A. Fisher and Rohan Dharmakumar

Sci Transl Med **11**, eaat4407.
DOI: 10.1126/scitranslmed.aat4407

BOLD-hearted

Atherosclerosis and other conditions can restrict the flow of blood to the heart, resulting in tissue damage and ischemic heart disease (IHD). Yang *et al*. used repeat hypercapnia (transient elevation in carbon dioxide) during cardiac magnetic resonance imaging to detect myocardial oxygenation in a model of IHD in canines. Without relying on exogenous contrast agents, this blood oxygen level–dependent (BOLD) imaging method could map regions of the heart affected by coronary narrowing. Combined with a computational framework that reduces noise, the authors demonstrated the ability to perform noninvasive, rapid, whole-heart imaging under free-breathing conditions, suggesting that this technique may be useful for monitoring myocardial ischemia.